JJMIE

Volume 15, Number 4, October. 2021
ISSN 1995-6665
Pages 347 - 355

Jordan Journal of Mechanical and Industrial Engineering

Control of Wake Behind an Unconfined Wedge Structure by Magnetohydrodynamics

Shailendra Rana[a*], Hari B. Dura, Rajendra Shrestha

Department of Mechanical and Aerospace Engineering, Pulchowk Campus, Institute of Engineering, Tribhuwan University, Kathmandu 00977, Nepal

Received July 7 2020 *Accepted August 14 2021*

Abstract

The laminar, viscous and incompressible flow of an electrically conducting fluid across an unconfined wedge structure in the presence of a transverse magnetic field has been studied. Two-dimensional numerical simulations have been performed for Reynolds number (*Re*) = 1-150 and Hartmann number (*Ha*) = 0-10 for a fixed blockage ratio *(β) = d/W* = 1/30. The magnetic induction method in magnetohydrodynamics module built in ANSYS FLUENT solver has been employed to compute the flow fields. Results show that the vortex shedding can be completely eliminated if the applied magnetic field is strong enough. In the steady flow regime, it has been found that the recirculation length reduces with the increase in *Ha*. A minimal reduction in the drag coefficient is observed with the increase in *Ha* as long as unsteady flow is maintained (*Ha* < 7.3). However, the drag coefficient has a tendency to significantly increase with the increase in *Ha* for steady flow. Similarly, the lift amplitude decreases with the increase in Ha indicating a diminishing effect on the strength of vortices. A critical Hartmann number (*Hacr*) of 7.3 has been found for *Re* = 100 at which complete suppression of vortex shedding is observed.

Keywords: Magnetohydrodynamics, active vortex suppression, Strouhal number, magnetic Reynolds number, Hartmann number;

1. Introduction

Studies on bluff bodies have been extensively carried out because of their complex flow dynamics and relevance to practical engineering problems [1-4]. Examples of the engineering applications include heat exchangers, pipelines, offshore marine structures, high-rise buildings etc. Commonly used bluff bodies for numerical and experimental studies are circular, square or rectangular cylinders. These bodies, irrespective of their geometry, present many similarities in terms of wake structure at different Reynolds numbers. One important characteristic regarding the flow around these bodies is the unsteady periodic vortex shedding phenomena occurring at a particular Reynolds number. Under such flow conditions, these bluff bodies experience unsteady forces which may cause fatigue damage due to flow-induced vibrations. The unsteady forces acting on these bodies can be reduced by controlling the vortex shedding phenomena through several flow control techniques. Examples of such flow control techniques are electrical methods, use of thermal effects, geometrical modifications such as grooves, rotary oscillations, magnetohydrodynamics, etc. A comprehensive review of several active and passive control methods employed for the control of flow-induced vibrations was given by Rashidi et al. [5].

Among several flow control techniques, the concept of magnetohydrodynamics (MHD) has been exploited by many industries to control and manipulate the flow of electrically conducting fluids, such as liquid metals, electrolytes, etc. The concept is that the motion of an electrically conducting fluid under the influence of an external magnetic field induces electric currents, which interacts with the magnetic field to produce Lorentz force [6]. This force has a dampening effect on the flow structure.

Vortex dynamics has been the subject of great interest to researchers for many years. Oyewola et al. [7] numerically investigated the effects of spacing ratios (*S/D* = 1.1, 1.1, 1.8, 2.0, 2.2, 2.4, 3.0, 4.0 and 5) on the forced convection flow of air at *Re* = 23500 over a pair of circular cylinders in tandem arrangement. They found that the increase in spacing ratios augments the local Nusselt number on the four portions of the cylinders. Bouakkaz et al. [8] studied the two-dimensional unsteady flow and heat transfer of water-based Cu nanofluid over a square cylinder considering nanoparticle volume fractions and angle of inclination in the range of 0-5% and 0-450 respectively. They concluded that the local Nusselt number increases with the rise in nanoparticle volume fraction for a fixed inclination angle. In the past, several works regarding the control of vortex shedding past bluff bodies using different techniques have been done. Hafsia and Nouri [9] investigated the effects of grooves and permeable plates on vortex shedding over a single circular cylinder at *Re* = 20 and 100. They found that the vortex shedding is considerably suppressed under the influence of two grooves and two permeable plates. Besides this, researchers have also shown keen interest in studying vortex dynamics using MHD. Singha et al. [10] investigated the laminar viscous flow of a conducting fluid past a square cylinder under the influence of transverse magnetic field at Reynolds numbers from 50 to 250. It was found that the size of the recirculation region behind the cylinder diminishes with the increment in

* Corresponding author e-mail: ranashailendra74@gmail.com

the magnetic field for a steady flow. Within the unsteady flow regime, a minimal increment in the Strouhal number was observed and the reduction in the amplitude of lift coefficient was observed implying that the strength of shed vortices has diminished. It was also concluded that the complete elimination of vortex shedding is achievable and steady flow could be attained if the applied magnetic field is strong enough. Singha and Sinhamahapatra [11] investigated the effect of transversemagnetic field on vortex shedding past a circular cylinder placed in a channel at *Re* = 50-250. The size of the recirculation zone formed behind the cylinder reduces with the increase in the strength of magnetic field. Also, a critical Hartmann number at *Re* = 250 was found to be 5.5. Farjallah et al. [12] studied the heat transfer and vortex shedding past a bounded square obstacle for *Re* = 80-250 and *Ha* = 0-4 at a fixed blockage ratio (β) = 1/4. Their results showed that the magnitude of drag and lift coefficients decrease on the application of magnetic field. They also found that at *Re* = 200, the periodic vortex shedding phenomena transitions to steady flow for *Ha* = 4. Chatterjee et al. [13] investigated the flow of a conducting fluid past circular and square cylinders in an unconfined medium for low *Re* = 10-40 and *Ha* = 0-10 at a blockage ratio (β) = 1/20 to control the steady separated flow using finite volume method. Their findings showed that the recirculation length and the separation angle decrease with the increase in *Ha*. Drag coefficient was found to increase with the increase in the magnitude of magnetic field. Chatterjee and Chatterjee [14] numerically analyzed the forced convection heat transfer past a circular cylinder for *Re* = 10-80 and *Ha* = 0-10 at a fixed blockage ratio (β) = 1/4 using ANSYS FLUENT. They considered three different working fluids having Prandtl number, *Pr* = 0.02 (liquid metal), 0.71 (air) and 7 (water) to analyze the heat transfer phenomena under the presence of transverse or aligned magnetic field. Their study concluded that the recirculation region gets suppressed at a faster rate for transverse magnetic field in comparison to aligned magnetic field. A significant increment in the drag coefficient for lower *Re* was observed and found to be more pronounced for transverse magnetic field in comparison with the aligned magnetic field. The Nusselt number was found to increase with Reynolds number and also with Hartmann numbers for a transverse magnetic field. Esfahani [15] employed finite volume method to study the effects of streamwise magnetic field on vortex shedding and wake structure behind a solid circular obstacle placed in a rectangular channel at *Re* = 1-200 and Stuart number (*N*) = 0-10. Their study concluded that at *N* = 4, the flow stabilizes as evidenced by the transition from unsteady flow pattern with vortex shedding to the steady state with symmetric recirculation bubbles. They also observed that the drag coefficient decreases for *N* < 0.22 whereas it increased rapidly for higher values of *N* (i.e. *N*=5). Rashidi et al. [16] performed a numerical investigation regarding the control of wake structure past a square cylinder confined in a rectangular channel under the streamwise magnetic field for *Re* = 1-250 and *N* = 0 -10 using finite volume method. Their results showed that the Strouhal number decreases linearly with the increase in *N*. Also, the flow pattern changes from time-dependent with vortex shedding to the steady state with the increase in *N*. Recently, Hussam et al. [17] numerically investigated the effects of axial magnetic field on the fluid flow and heat transfer of Galinstan (GaInSn) eutectic alloy past a confined triangular cylinder at *Re* = 100-3000 and *Ha* = 100-2400 for a blockage ratio (β) = 1/4. They found triangular cylinder to be superior promoter geometry in terms of heat transfer augmentation compared to the square or circular cylinders. From the review of above literature, it is evident that magnetohydrodynamics is an efficient technique to control the flow past bluff bodies. It can also be concluded that the shape of an obstacle has a significant influence on the flow dynamics. Like circular and square-shaped bodies, triangular cylinders also exhibit the periodic vortex shedding phenomena. Moreover, the presence of highly sharped corners in triangular cylinders in comparison to circular or square cylinders contributes to more intense hydrodynamic instabilities. Such intense instabilities, therefore, require stronger magnetic fields for flow suppression [13].

Previous research works mentioned in the paper indicate that limited research works have been done regarding the control of flow around triangular cylinder using magnetic field. To the best of authors' knowledge, there are no reported works done regarding the control of vortex shedding and wake structure past triangular cylinders using magnetohydrodynamics in an unconfined medium at low Reynolds numbers. The low Reynolds numbers considered in this study i.e. *Re* = 1-150 are evident in microfluidic applications and in liquid metal flows in nuclear reactors and semi-conductors. Also, the turbulence created by triangular cylinders is essential to heat transfer enhancement. Moreover, this work will further supplement to the existing knowledge regarding magnetohydrodynamic flows over bluff bodies. Hence, this paper investigates the effects of magnetic field on vortex shedding and wake structure behind the triangular cylinder (wedge) in an unconfined medium at low Reynolds and Hartmann numbers.

2. Problem Description and Mathematical Modelling

2.1. Geometrical configuration

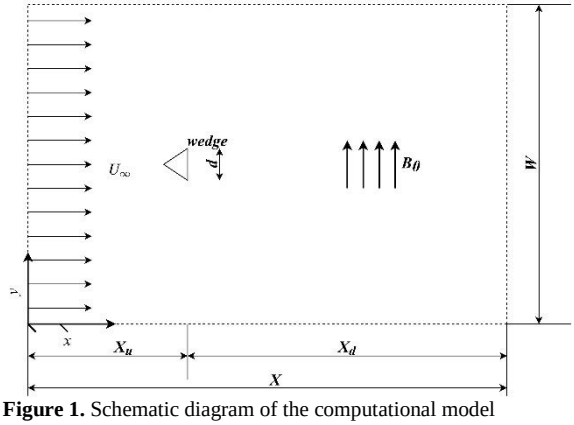

Figure 1. Schematic diagram of the computational model

The geometrical configuration for the current research is shown in Figure 1. Two-dimensional laminar incompressible viscous flow of an electrically conducting fluid having constant electrical conductivity (σ), kinematic viscosity(η)and density (ρ) across a wedge structure of side length (*d*) is considered. The wedge is an equilateral triangular cylinder placed in an unconfined medium.

However, to create a finite computational domain, the blockage ratio, $\beta = d/W$ =1/30 is set as per the domain independency test conducted by [2]. To simulate the unconfined flow, a free-slip boundary condition is assigned on the upper and lower walls of the computational domain. The fluid flow with free stream velocity (U_∞) in the presence of an external magnetic field (B_0) in a transverse direction is considered. All the solids walls are insulated. Table 1 gives the value of the normalized dimensions of the physical domain used in this study.

Table 1. Geometrical details

S.N.	Geometrical parameters	Dimensions
1	Upstream length (X_u/d)	12
2	Downstream length (X_d/d)	20
3	Total axial length (X)	32
4	Domain height (W/d)	30

2.2. Governing equations

Two-dimensional laminar unsteady flow of an incompressible conducting fluid with constant properties in the presence of a transverse magnetic field is considered. Under such assumptions, the dimensionless governing equations of conservation of mass and momentum can be expressed as follows [13]:

Conservation of mass:

$$\nabla . V = 0 \quad (1)$$

Conservation of momentum:

$$\frac{\partial V}{\partial \tau} + (V.\nabla)V = -\nabla P + \frac{1}{Re}\nabla^2 U + \frac{Ha^2}{Re}(J \times B) \quad (2)$$

Here, the term $J \times B$ represents the Lorentz force acting in the computational domain.

The derivation of the dimensional form of the magnetic induction equation is as follows:

Maxwell's equations:

$$\nabla . \mathrm{B} = 0 \quad (3)$$

$$\nabla \times \mathrm{E} = -\frac{\partial \mathrm{B}}{\partial \mathrm{t}} \quad (4)$$

$$\nabla . \mathrm{D} = \mathrm{q} \quad (5)$$

$$\nabla \times \mathrm{H} = \mathrm{J} + \frac{\partial \mathrm{D}}{\partial \mathrm{t}} \quad (6)$$

The induction fields H and D can be expressed as follows:

$$\mathrm{H} = \frac{1}{\mu_0}\mathrm{B} \quad (7)$$

$$\mathrm{D} = \varepsilon \mathrm{E} \quad (8)$$

where ε is the electric permittivity and E is the electric field.

According to Ohm's law, the current density can be defined as:

$$\mathrm{J} = \sigma \mathrm{E} \quad (9)$$

If the fluid is moving with velocity field u in the presence of magnetic field B, the current density becomes,

$$\mathrm{J} = \sigma(\mathrm{E} + \mathrm{u} \times \mathrm{B}) \quad (10)$$

Using Eq. 4,

$$\frac{\partial \mathrm{B}}{\partial \mathrm{t}} = -\nabla \times \mathrm{E} \quad (11)$$

From Eq. 10,

$$\mathrm{E} = \frac{\mathrm{J}}{\sigma} - \mathrm{u} \times \mathrm{B} \quad (12)$$

Applying curl both sides in Eq. (12), we get,

$$\nabla \times \mathrm{E} = \nabla \times \left(\frac{\mathrm{J}}{\sigma} - \mathrm{u} \times \mathrm{B}\right) \quad (13)$$

Combining Eqs. (11) and (13),

$$\frac{\partial \mathrm{B}}{\partial \mathrm{t}} = -\nabla \times \left(\frac{\mathrm{J}}{\sigma} - \mathrm{u} \times \mathrm{B}\right) \quad (14)$$

$$\frac{\partial \mathrm{B}}{\partial \mathrm{t}} = -\nabla \times \left(\frac{\mathrm{J}}{\sigma}\right) + \nabla \times (\mathrm{u} \times \mathrm{B}) \quad (15)$$

Neglecting the displacement current in Eq. 6, we obtain,

$$\nabla \times \mathrm{H} = \mathrm{J} \quad (16)$$

Inserting Eq. 7 into Eq. 16,

$$\frac{\nabla \times \mathrm{B}}{\mu_0} = \mathrm{J} \quad (17)$$

After substitution of Eq. 17 into Eq. 15, we obtain,

$$\frac{\partial \mathrm{B}}{\partial \mathrm{t}} = -\nabla \times \left(\frac{1}{\mu_0 \sigma}(\nabla \times \mathrm{B})\right) + \nabla \times (\mathrm{u} \times \mathrm{B}) \quad (18)$$

Eq. 18 can be rewritten as,

$$\frac{\partial \mathrm{B}}{\partial \mathrm{t}} = -\frac{1}{\mu_0 \sigma}\nabla \times (\nabla \times \mathrm{B}) + \nabla \times (\mathrm{u} \times \mathrm{B}) \quad (19)$$

After a few mathematical operations, Eq. 19 can be expressed as follows:

$$\frac{\partial \mathrm{B}}{\partial \mathrm{t}} = -\frac{1}{\mu_0 \sigma}\big(\nabla(\nabla . \mathrm{B}) - \mathrm{B}(\nabla . \nabla)\big) + \mathrm{u}(\nabla . \mathrm{B}) - \mathrm{B}(\nabla . \mathrm{u}) \quad (20)$$

Using Eq. 3, we get,

$$\frac{\partial \mathrm{B}}{\partial \mathrm{t}} = \frac{1}{\mu_0 \sigma}\nabla^2 \mathrm{B} + \mathrm{u}(\nabla . \mathrm{B}) - \mathrm{B}(\nabla . \mathrm{u}) \quad (21)$$

Finally, rearranging Eq. 21, we obtain,

$$\frac{\partial \mathrm{B}}{\partial \mathrm{t}} + \mathrm{B}(\nabla . \mathrm{u}) = \frac{1}{\mu_0 \sigma}\nabla^2 \mathrm{B} + \mathrm{u}(\nabla . \mathrm{B}) \quad (22)$$

Eq. 22 represents the dimensional form of the magnetic induction equation derived from Ohm's law and Maxwell's equations.

The present calculations show that the magnetic Reynolds number, $Re_m = \mu_0 \sigma U_\infty d$, is in the order of 10^{-4}. Since $Re_m << 1$, the magnitude of induced magnetic field b is negligible in comparison to the total magnetic field B [18]. The Reynolds and Hartmann numbers have been defined on the basis of side length of the wedge as:

$$Re = \frac{U_\infty d}{\eta} \quad (23)$$

$$Ha = B_0 d \sqrt{\frac{\sigma}{\eta \rho}} \quad (24)$$

2.3. Grid structure and numerical details

Structured non-uniform grids have been generated using ICEM CFD software. The grid structure is shown in Figure 2 (a). The grid refinement around the vicinity of wedge is shown in Figure 2 (b). The grid used in this study consists of 114147 cells having 200 grid points on each side of the wedge. For grid resolution study, three progressively refined grids have been generated namely: G1, G2 and G3 each are having 114147 cells with size of the first grid point from the triangular body of 0.004d, 0.0015d and 0.001d units respectively.

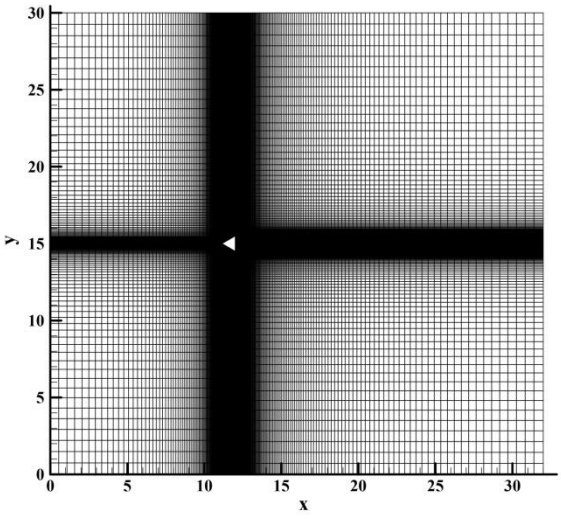

(a)

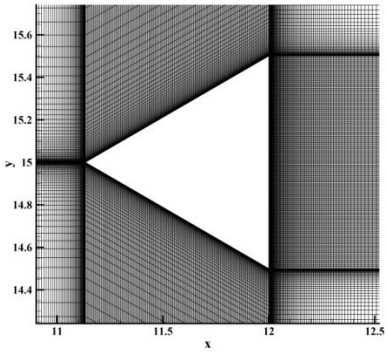

(b)

Figure 2. Grid structure: (a) Full view, (b) Zoomed view

In the present work, ANSYS FLUENT code based on finite volume method has been employed to carry out all numerical simulations. The magnetic induction method in MHD module built in ANSYS FLUENT has been used to simulate MHD flows. The SIMPLE (Semi-implicit Method for Pressure Linked Equations) algorithm is used for coupling between continuity and momentum equations. The second-order implicit scheme has been utilized for temporal discretization. For spatial discretization, the second-order upwind scheme has been used for convective terms while the central difference scheme has been employed for diffusive terms. A convergence criterion of 10^{-6} has been set.

The boundary conditions associated with the physical problem shown in Figure 1 are explained as follows:

1. *At the inlet plane:* A uniform fluid flow in free-stream condition is considered, that is, $u = 1$, $v = 0$. *Velocity inlet* condition has been assigned at the inlet boundary.
2. *On the top and bottom walls:* Since the present study considers an unconfined flow across the wedge, a *free slip* condition has been applied on the top and bottom boundaries of the flow domain.
3. *On the surface of wedge: No-slip* condition has been applied on the solid surface of the wedge, that is, $u = 0$, $v = 0$.
4. *At the exit plane: Pressure outlet* condition has beenapplied at the exit boundary.

2.4. Grid resolution study

For grid resolution study, simulations have been performed at $Re = 150$ with a time step size, $\Delta t = 0.01$ s using the three progressively refined grids namely: G1, G2 and G3. The results of grid resolution study are shown in Table 2. Table 2 shows the variation in the values of the drag coefficient (C_d) and the Strouhal number (St) for the aforementioned grids. It is observed that the percentage differences in the values of the mean drag coefficient and the Strouhal number between G1 and G3 grids are found to be 0.27% and 5.21% respectively. Similarly, for G2 and G3 grids, the percentage difference in the value of the mean drag coefficient has been found to be 0.05%, but no further changes in the Strouhal number has been observed. Hence, G2 grid with $\lambda = 114147$ cells and $\Delta = 0.0015d$ has been selected for the rest of the simulations.

Table 2. Grid resolution study at $Re = 150$

Grid	λ	Δ	C_d	St
G1	114147	0.004d	1.9188	0.211
G2	114147	0.0015d	1.9231	0.2
G3	114147	0.001d	1.9240	0.2

3. Results and Discussion

3.1. Non-MHD flows (Ha = 0)

3.1.1. Validation

A comparative analysis of the present numerical results of the drag coefficient and the Strouhal number against the published results of [1] and [2] has been done at Re = 10-150. An excellent agreement between the present results and the published literature of time-averaged drag coefficient at $Re = 50$, 100 and 150 has been obtained as shown in Figure 3. It is seen that the average difference between the present results and the published literature of time-averaged drag coefficient at $Re = 50$, 100 and 150 is 1.23%. Figure 4 shows the comparison of the present results of Strouhal number at $Re = 50$, 100 and 150 against the published literature. An excellent agreement between the present results and the published results of Strouhal number has been obtained. It is seen that the average difference between the present results and the published data of the Strouhal number is 2.32%.

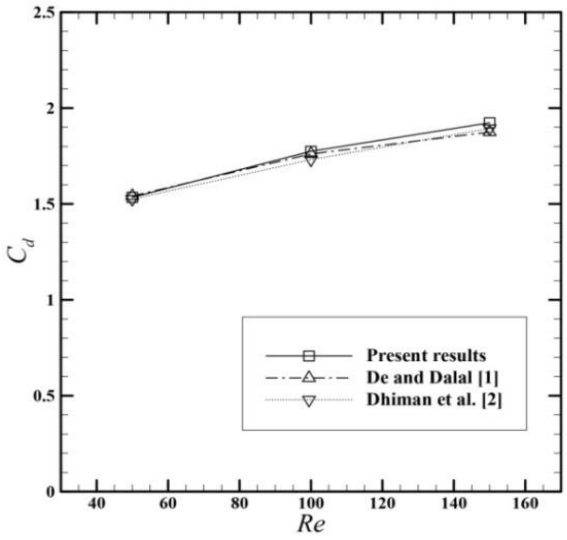

Figure 3. Validation of time-averaged C_d at Re = 150 (Ha = 0)

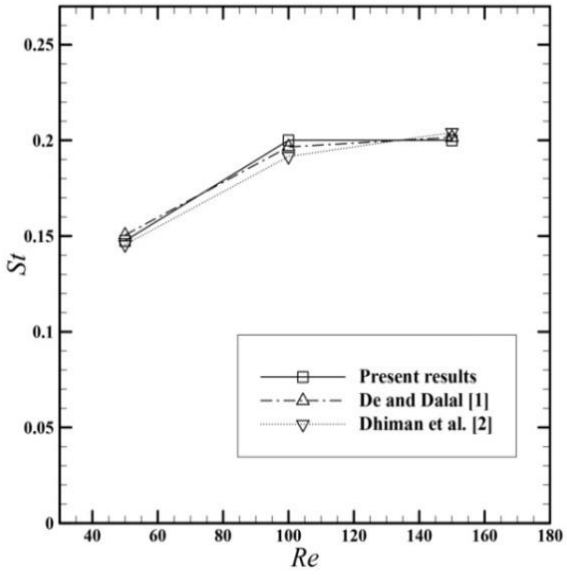

Figure 4. Validation of St at Re = 150 (Ha = 0)

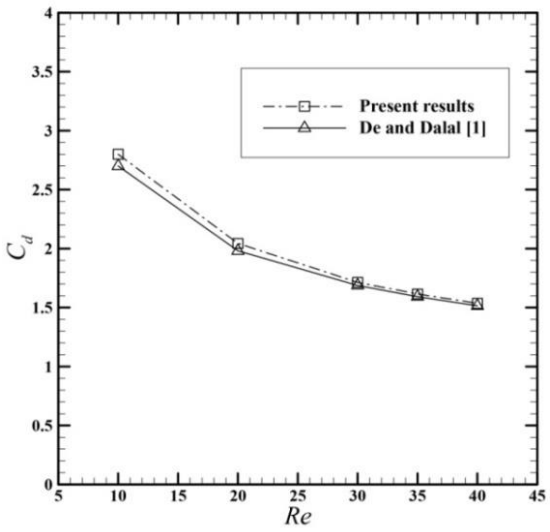

Figure 5. Validation of C_d at Re = 10-40 (Ha = 0)

Also, the drag coefficient for Re = 10 - 40 has been computed and compared with the data reported by the literature. An excellent agreement has been obtained between the present results and the published results of drag coefficient as shown in Figure 5. It is observed that the average difference between the present results and that of published literature of drag coefficient is 2.24%. Hence, non-MHD tests validate the present numerical solutions.

3.1.2. Flow structures

The flow around the wedge in the absence of magnetic field has been studied. The streamlines and vorticity contours for Re = 1, 10, 30 and 100 around the wedge in the absence of magnetic field are depicted in Figures 6 and 7. At low Reynolds number i.e. Re = 1, the fluid particles attaches to the surface of the wedge due to dominant viscous forces compared to the inertial forces and a creeping motion of the fluid with no flow separation isobserved as shown in Figure 6 (a). For Re = 10 and 30, the flow separates due to adverse pressure gradient, forming a closed steady recirculation zone behind the wedge consisting of symmetric twin vortices, also known as 'recirculation bubbles' as shown in Figures 6 (a). At Re = 100, the vortex shedding phenomenon begins to take place and vortices shed from the upper and the lower regions of the wedge as shown in Figure 7 (b).

3.2. MHD flows

3.2.1. Flow structures

The influence of magnetic field on the flow around the wedge at Re = 30 and 100 and Ha = 0 - 10 has been investigated. The magnetic field applied in a transverse direction produces a resistive force known as Lorentz force in the upstream direction which can alter the wake structure. Figure 8 shows the streamlines at Re = 30 in the presence of magnetic field. At Ha = 0 (i.e. without magnetic field), the flow at Re = 30 can be considered as purely hydrodynamic, characterized by the presence of closed steady symmetric recirculating bubbles formed behind the wedge as shown in Figure 8 (a).It is observed that the size of the recirculation bubbles decreases with the increase in Hartmann number as depicted in Figures 8 (a-c). As the Hartmann number is further increased, the recirculation bubbles disappear and a creeping flow structure with no flow separation is observed as shown in Figure 8 (d). Figures 9 and 10 show the streamlines and vorticity contours at Re = 100 under different strengths of magnetic field (Ha = 0 - 10). At Ha = 0, the flow is unsteady with the presence of alternate shedding of vortices from the upper and the lower regions of the wedge. At Ha < 7.3, the flow remains in the unsteady state evidenced by the presence of alternate shedding of vortices as shown in Figures 9 (a-c) and Figures 10 (a-c). However, at Ha = 7.3, the shedding of vortices is completely eliminated and the flow transitions to steady state forming a wake consisting of closed symmetric recirculation bubbles as shown in Figure 9 (d).As the Hartmann number is further increased, the size of the recirculation bubbles decreases due to dampening effect caused by the Lorentz force as shown in Figures 9 (d-e).

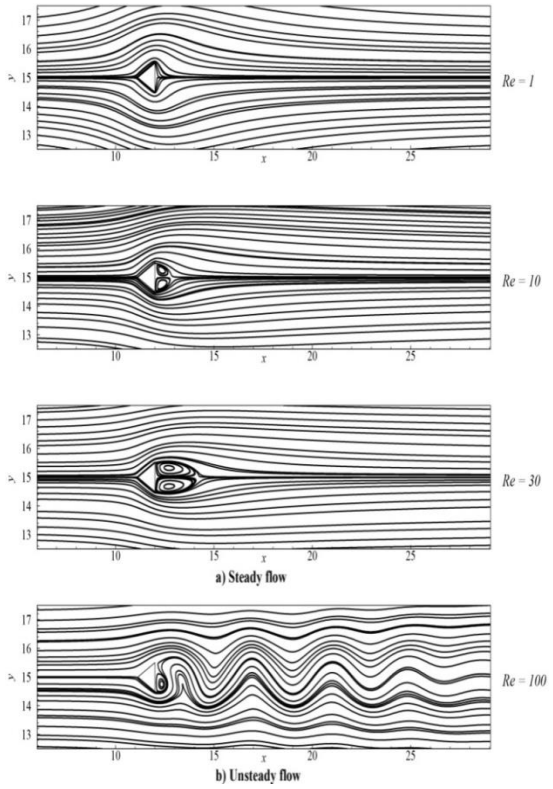

Figure 6. Streamlines: (a) Steady flow (*Re* = 1, 10, 30), (b) Unsteady flow (*Re* = 100, t = 220 s)

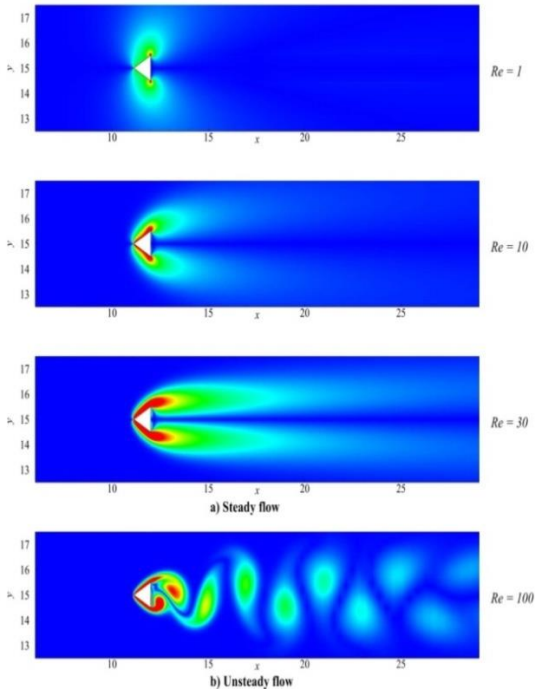

Figure 7. Vorticity contours: (a) Steady flow (*Re* = 1, 10, 30), (b) Unsteady flow (*Re* = 100, t = 220 s)

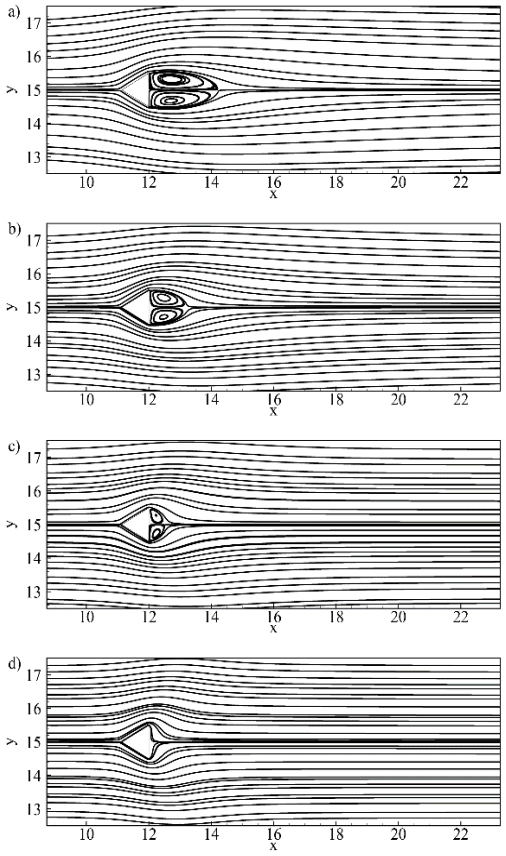

Figure 8. Streamlines for *Re* = 30: (a) *Ha* = 0, (b) *Ha* = 2, (c) *Ha* = 5, (d) *Ha* = 10

3.2.2. Influence on drag and lift coefficients

Figures 11 (a–e) show the temporal variation of the drag coefficient at *Re* = 100 for various Hartmann numbers. The drag coefficient is found to decrease up to certain Hartman numbers as long as the flow remains in unsteady flow regime as shown in Figures 11 (a-c).

Such drop in drag coefficient may be attributed to the decrease in forces due to shear stress with the increase in Hartmann number within the unsteady flow regime. However, once the flow assumes the steady state at *Ha* = 7.3, the drag coefficient has a tendency to increase with a further increase in Hartmann number (i.e. *Ha* = 10). The possible explanation is that with further increase in Hartmann number, the velocity field is significantly suppressed, causing the boundary layer thickness to increase and hence the drag. The temporal variation of the lift coefficient for *Re* = 100 at different Hartmann numbers is shown in Figures 12 (a-e). As the Hartmann number is increased, the amplitude of lift coefficient is decreased, implying the reduction in strength of shed vortices as shown in Figures 12 (a-c). With further increase in Hartmann number, the lift coefficient is zero indicating that the flow has attained steady state as shown in Figures 12 (d-e).

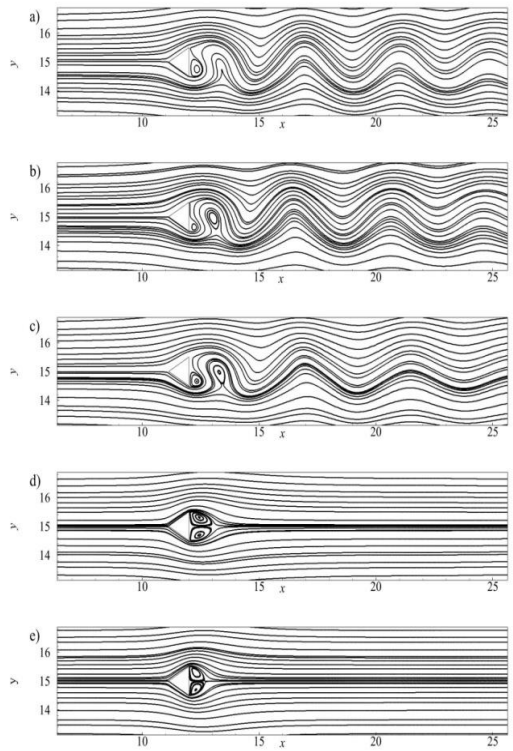

Figure 9. Instantaneous streamlines at *Re* = 100: (a) *Ha* = 0, t = 220 s, (b) *Ha* = 2, t = 203 s (c) *Ha* = 5, t = 217 s (d) *Ha* = 7.3, (e) *Ha* = 10

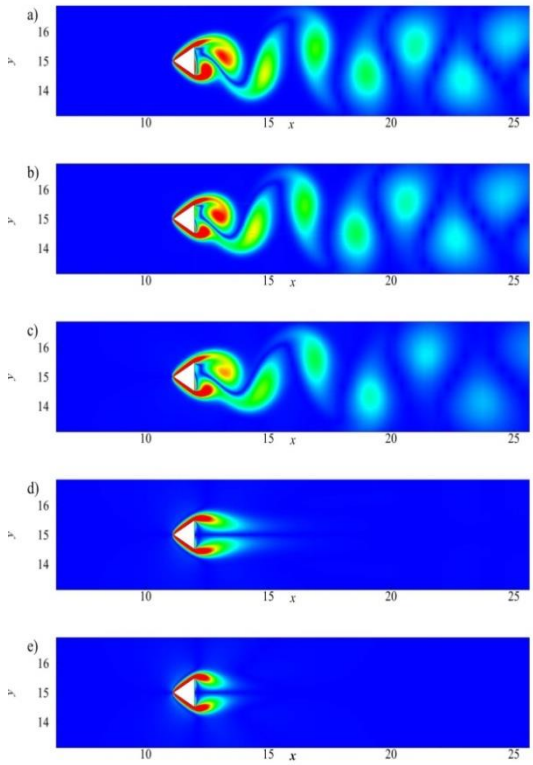

Figure 10. Instantaneous vorticity contours at *Re* = 100: (a) *Ha* = 0, t = 220 s, (b) *Ha* = 2, t = 203 s (c) *Ha* = 5, t = 217 s (d) *Ha* = 7.3, (e) *Ha* = 10

3.2.3. Critical Hartmann number

Critical Hartmann number refers to the minimum value of magnetic field at which the vortex shedding is completely suppressed and a steady and symmetric flow is established. Such value is dependent on several factors such as shape of obstacle, blockage ratio, Reynolds number, etc. The present result of the critical Hartmann number for the wedge has been compared with the published data of circular and square cylinders.

Table 3. Published results of critical Hartmann number for different bluff bodies

Re	Square cylinder (Singha et al. [7])	Circular cylinder (Singha et al. [8])	Square cylinder (Farjallah et al. [9])
100	-	-	1.272
150	2.0-2.5	2.0-2.5	-
200	3.5-4.0	4.0-4.5	-
250	4.5-5.0	5.0-5.5	-

The values of critical Hartmann number at *Re* = 100 - 250 for confined square and circular cylinders with their blockage ratios (β) = 1/4 is provided in Table 3. It can be observed that with the rise in Reynolds number, the critical Hartmann number increases for both square and circular cylinders at a fixed blockage ratio. This can be explained by the fact that the inertial forces increase with the increment in Reynolds number, requiring higher strengths of magnetic field. In the present work, the flow over the wedge in an unconfined condition is considered. Under such condition, at *Re* = 100, the value of the critical Hartmann number has been found to be 7.3. A comparison of the present results of the critical Hartmann number has been made against the published resuls of Farjallah et al. [9]. In his work, he developed a theoretical correlation, $Ha_{cr} = 0.0239Re - 1.118$ for a confined square cylinder which characterizes the relationship between critical

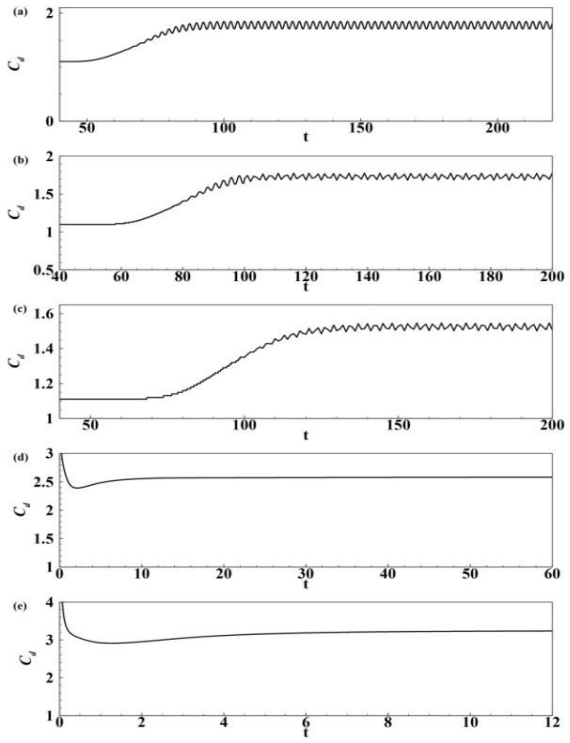

Figure 11. Temporal variation of drag coefficient at *Re* = 100: (a) *Ha* = 0, (b) *Ha* = 2.0, (c) *Ha* = 5.0, (d) *Ha* = 7.3, (e) *Ha*= 10

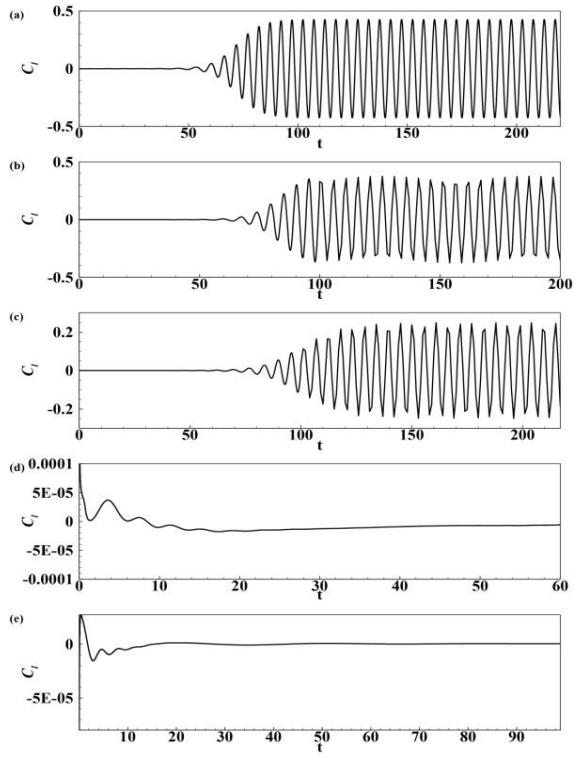

Figure 12. Temporal variation of lift coefficient at *Re* = 100: (a) *Ha* = 0, (b) *Ha* = 2.0, (c) *Ha* = 5.0, (d) *Ha* = 7.3, (e) *Ha* = 10

Hartmann number and Reynolds number. In comparison to the value of Ha_{cr} = 1.272, it can be observed that the value of Ha_{cr} for the wedge is much larger. This may be atttributed to the fact that the wedge consists of sharply defined corners, leading to intense flow instabilities and thus, requires stronger magnetic field [13]. In addition, it isnoteworthy that at high blockage ratios, the wall boundary layer has a stabilizing effect on the flow in such a way that it can inhibit vortex shedding around bluff bodies [19]. But in our case, the presence of walls at a larger distance has no influence on regular formation of vortex shedding past the wedge and thus, contributes to more magnetic field requirements.

4. Conclusions

In this paper, a laminar incompressible viscous flow of an electrically conducting fluid past a wedge in an unconfined medium in the presence of transverse magnetic field has been studied. The magnetic induction method in MHD module built in ANSYS FLUENT has been considered to carry out all MHD simulations. The conclusions drawn from this study are enumerated below:

1. If the magnetic field is strong enough, the complete elimination of vortex shedding is achievable.
2. A critical Hartmann number, Ha_{cr} = 7.3 has been found at *Re* = 100, at which complete elimination of vortex shedding is observed.
3. In the steady flow regime, the length of the recirculation zone reduces with the increment in *Ha*.
4. A minimal reduction in the drag coefficient has been observed for unsteady flow regime (i.e. *Ha* < 7.3). However, once the flow attains steady state at *Ha* = 7.3, it starts to significantly increase with a further increase in *Ha* (i.e. *Ha* = 10).
5. The reduction in lift amplitude is observed with the increment in *Ha*, indicating a diminishing effect in the strength of shed vortices.

5. Acknowledgements

All the computer simulations were carried out in the Computer-Aided Engineering Laboratory, Department of Mechanical and Aerospace Engineering, Pulchowk Campus. The authors extend their heartfelt gratitude to the department for their continuous support by providing access to computational facilities.

Nomenclature

b	induced magnetic field	T
B	non-dimensional total magnetic field	
B	total magnetic field	T
B_0	external magnetic field	T
C_d	drag coefficient	
C_l	lift coefficient	
E	electric field	Vm^{-1}
H	magnetic field strength	Am^{-1}
D	electric displacement field	Cm^{-2}
q	charge density	Cm^{-3}
Ha	Hartmann number	
Ha_{cr}	critical Hartmann number	
Pr	Prandtl number	
J	current density	Am^{-2}
J	non-dimensional current density	
N	Stuart number	
Re	Reynolds number	
Re_m	magnetic Reynolds number	
St	Strouhal number	
τ	non-dimensional time	
t	dimensional time	s
u	dimensional velocity field	ms^{-1}
U_∞	freestream velocity	ms^{-1}
u	non-dimensional x-velocity	
V	non-dimensional velocity field	
v	non-dimensional y- velocity	
W	height of the domain	m
X	total length of the domain	m
X_u	upstream length of the domain	m
X_d	downstream length of the domain	m
D	diameter of cylinder	m
S	spacing between centres of cylinder	m
q	charge density	
x	stream-wise co-ordinate	m
y	transverse co-ordinate	m
Δt	time-step size	s

Greek symbols

β	blockage ratio	
Δ	first cell height	m
λ	total number of cells	
μ_0	magnetic permeability	Hm^{-1}
η	kinematic viscosity	m^2s^{-1}
ρ	density	kgm^{-3}
σ	electrical conductivity	Sm^{-1}

References

[1] A.K. De, A. Dalal, "Numerical simulation of unconfined flow past a triangular cylinder". International Journal for Numerical Methods in Fluids, Vol. 52, No. 7, 2006, 801-821.

[2] A. Dhiman, R. Shyam, "Unsteady heat transfer from an equilateral triangular cylinder in the unconfined flow regime". ISRN Mechanical Engineering, Vol. 2011, Feb., 2011, 1-13.

[3] B.N. Rajani, A. Kandasamy, S. Majumdar, "Numerical simulation of laminar flow past a circular cylinder". Applied Mathematical Modelling, Vol. 33, No. 3, 2009, 1228-1247.

[4] P. Catalano, M. Wang, G. Iaccarino, P. Moin, "Numerical simulation of the flow around a circular cylinder at high Reynolds numbers". International Journal of Heat and Fluid Flow, Vol. 24, No. 4, 2009, 463-469.

[5] S. Rashidi, M. Hayatdavoodi, J.A. Esfahani, "Vortex shedding suppression and wake control: A review". Ocean Engineering, Vol. 126, Aug., 2016, 57-80.

[6] Davidson PA. An Introduction to Magnetohydrodynamics. 1st ed. Cambridge, United Kingdom: Cambridge University Press; 2001.

[7] O.M. Oyewola, O.S. Ismail, K. Abu, "Numerical simulation of forced convection flows over a pair of circular cylinders in tandem arrangement". Jordan Journal of Mechanical and Industrial Engineering, Vol. 13, No. 4, 2019, 221-230.

[8] R. Bouakkaz, Y. Khelili, F. Salhi, "Unconfined laminar nanofluid flow and heat transfer around a square cylinder with an angle of incidence". Jordan Journal of Mechanical and Industrial Engineering, Vol. 13, No. 3, 2019, 191-196.

[9] Z. Hafsia, S. Nouri, "The effect of grooves and permeable plates on the control of vortex shedding behind a single circular cylinder". Journal of Advanced Research in Fluid Mechanics and Thermal Sciences, Vol. 66, No. 2, 2020, 32-48.

[10] S. Singha, K.P. Sinhamahapatra, S.K. Mukherjea, "Control of vortex shedding from a bluff body using imposed magnetic field". Journal of Fluids Engineering, Vol. 129, No. 5, 2007, 517-523.

[11] S. Singha, K.P. Sinhamahapatra, "Control of vortex shedding from a circular cylinder using imposed transverse magnetic field". International Journal of Numerical Methods for Heat and Fluid Flow, Vol. 21, No. 1, 2011, 32-45.

[12] H. Farjallah, H. Abbassi, S. Turki, "Vortex shedding of electrically conducting fluid flow behind square cylinder under magnetic field". Engineering Applications of Computational Fluid Mechanics, Vol. 5, No. 3, 2011, 349-356.

[13] D. Chatterjee, K. Chatterjee, B. Mondal, "Control of flow separation around bluff obstacles by transverse magnetic field". Journal of Fluids Engineering, Vol. 134**,** No. 9, 2012, 1-11.

[14] D. Chatterjee, K. Chatterjee, "Wall--bounded flow and heat transfer around a circular cylinder at low Reynolds and Hartmann numbers". Heat Transfer-Asian Research, Vol. 42, No. 2, 2013, 133-150.

[15] J.A. Esfahani, "Control of wake and vortex shedding behind solid circular obstacle by magnetohydrodynamics". Journal of Thermal Engineering, Vol. 1, No. 7, 2015, 593-597.

[16] S. Rashidi, M. Bovand, J.A. Esfahani, H.F. Oztop, R. Masoodi, "Control of wake structure behind a square cylinder by magnetohydrodynamics". Journal of Fluids Engineering, Vol. 137, No. 6, 2015, 1-8.

[17] W.K. Hussam, A.H.A. Hamid, Z.Y. Ng, G.J. Sheard, "Effect of vortex promoter shape on heat transfer in MHD duct flow with axial magnetic field". International Journal of Thermal Sciences, Vol. 134, Dec., 2018, 453-464.

[18] Shercliff JA. A Textbook of Magnetohydrodynamics. New York: Pergamon Press; 1965.

[19] D.A. Perumal, G.V.S. Kumar, A.K. Dass, "Numerical simulation of viscous flow over a square cylinder using lattice Boltzmann method". ISRN Mathematical Physics, Vol. 2012, 2012, 1-16.